Journal of the Magnetics Society of Japan Vol. 15 Supplement, No. S2 (1991)

INVESTIGATIONS ON CO-EVAPORATED Co-Cr FILMS FOR PERPENDICULAR RECORDING APPLICATIONS

Herma van KRANENBURG*, Cock LODDER*, Theo J.A. POPMA*, Koji TAKEI and Yasushi MAEDA****

* Mesa Research Institute, University of Twente, P.O. Box 217, 7500 AE Enschede, The Netherlands.
** NTT Basic Research Laboratories, Tokai, Ibaraki 319-11, Japan.

Abstract---The magnetic behaviour of co-evaporated Co-Cr is investigated. The existence of a process-induced compositional separation, generated by the special geometry of the opposing vapour beams, leads to enhanced perpendicular characteristics without the necessity of depositing the films at a raised substrate temperature. In this paper we present results of a thickness series ranging from 50 to 750 nm. The existence of highly pure Co regions has been proved by means of NMR analysis. The anisotropy of the films is discussed in relation to the texture and morphology of the films.

INTRODUCTION

Co-Cr is a promising candidate medium for high density recording. Its basic magnetic properties, such as magnetization, coercivity and anisotropy depend on the microstructural properties and chemical inhomogeneities like separation of Co and Cr. We started the experiments with co-evaporated films in order to understand these properties in relation to the deposition parameters and to investigate the possibility of exploiting the geometrical effect of two opposing vapour beams.

EXPERIMENTAL

Deposition of the films is carried out in a high vacuum system with 2 e-beam sources. The evaporation is done at a typical background pressure of 2.10^{-7} mbar. The Co and Cr vapour arrive at the substrate from opposing directions, see fig. 1.

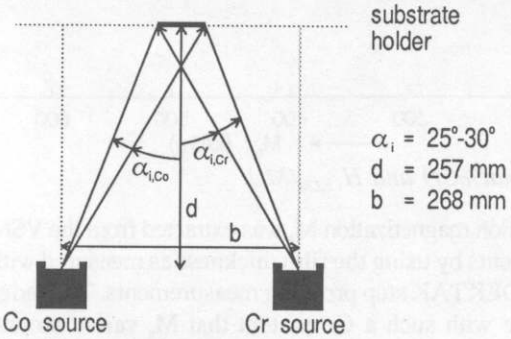

Fig. 1. Deposition geometry.

The substrate was located in the common evaporation plane (defined by the 2 vapour flux directions). The angle of incidence, α_i (defined between the film normal and vapour flux) at the centre position is $\alpha_{i,Co} = \alpha_{i,Cr} = 27.5°$. For a sample which has its centre 1 cm nearer to one of the sources (hereafter called off-centre samples), the incidence angle is 27.5°± 2°. We will discuss the differences between the centre and off-centre samples. The total deposition rate was 4 Å/s. The film thickness was varied between 50 and 750 nm. The thicker films were mainly used as an aid to understand the growth mechanism. One series was deposited at room temperature (T_R-samples). For comparison another series was deposited at high temperature (T_H-samples). The heating of the substrate was achieved with an infrared heater which was situated at a distance from the back of the substrate. The temperature near this heater, earlier called process temperature T_p [1], is measured. For the T_H-samples it was T_p=400°C. The actual substrate temperature is substantially lower. We used Si substrates. Before deposition the Si was cleaned with 2-propanol.

The magnetic properties were characterized by VSM and torque measurements. The VSM measurements were done both in the evaporation plane (LM measurement) and in the transversal plane (TM measurement), see fig 2. Most torque measurements were performed in the evaporation plane and in-plane.

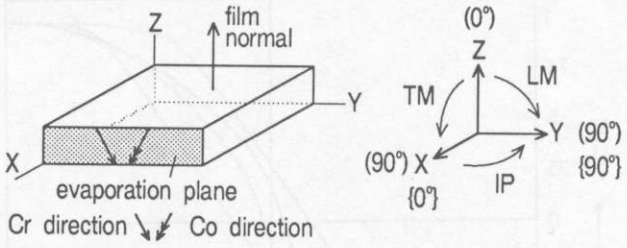

Fig. 2. Definition measurement planes. LM longitudinal, TM transversal and IP in-plane measurement. The angles between brackets are valid for TM and LM, those between parentheses for IP.

The morphology of the films was studied by high resolution SEM. We observed both the surface and the cross-section and measured the columnar dimensions and columnar inclination angle from it. The average Cr content was measured with XRF and EDS. With X-ray diffraction (XRD) θ-2θ scans

were made to determine the phase configuration. A texture diffractometer was used to measure the texture of the films. The cross-sectional model for the morphology as presented earlier [2] was now generated by a 2D-Monte Carlo simulation. We simulated the microstructure both at high and low surface diffusion. NMR experiments were carried out to analyse the Co and Cr distribution.

RESULTS AND DISCUSSION

Magnetization and coercivity.

Saturation hysteresis curves, as measured with VSM, are presented in fig. 3 for the 250 nm thick films. The perpendicular coercivities (i.e. angle between applied field and film normal is zero) are equal for both the LM and TM planes. For the T_R-samples a $H_{c\perp}$ of 50-60 kA/m is typical. For the

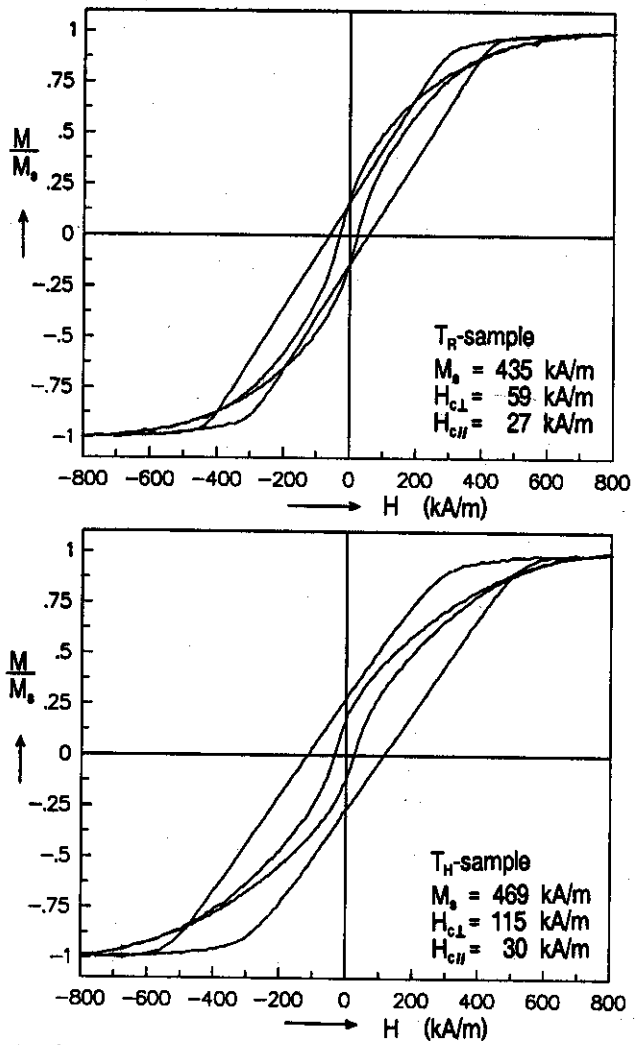

Fig. 3. MH-curves for the 250 nm thick centre samples; LM measurement.

T_H-samples a $H_{c\perp}$ around 90-110 kA/m. The in-plane coercivities are different for the LM and TM planes. The difference is caused by relative strong in-plane anisotropies.

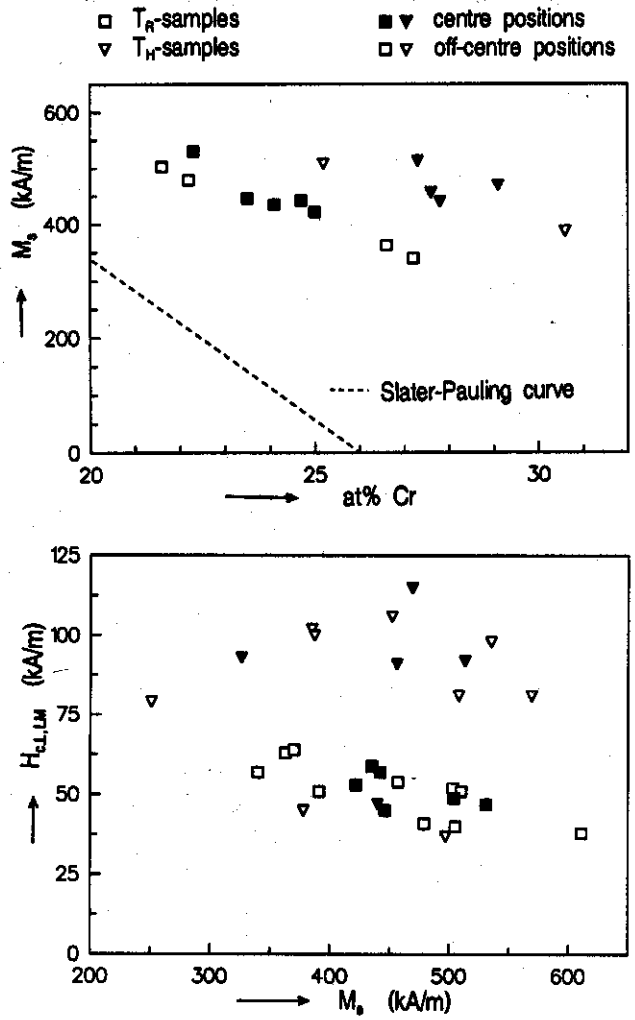

Fig. 4. M_s(at%Cr) and $H_{c\perp,LM}$(Ms).

The saturation magnetization M_s was extracted from the VSM measurements by using the film thickness as measured with XRF and DEKTAK step profiling measurements. The series were made with such a Cr content that M_s varied around 400-500 kA/m. For this we needed an average Cr content of appr. 25 at% for the T_R-samples and 28 at% for the T_H-samples. Off-centre samples had a Cr content of ± 2.5 at% and their film thicknesses differed from the centre samples by a factor 1.03. This is in agreement with a cosinus distribution of the vapour flux. Figure 4 combines coercivities, saturation magnetizations and Cr content. Saturation magnetizations are much higher than those for a homogeneous bulk Co-Cr layer (represented by the Slater-Pauling curve). Both series have a high $M_s \times H_{c\perp}$

product. The large M_s and $H_{c\perp}$ values are caused by separation into Co and Cr rich regions due to the special geometry of the opposing vapour beams. The Co vapour is responsible for most deposited atoms. Because of its oblique incidence arrival at the film surface, already deposited atoms will shadow adjacent regions from direct impingement of more Co atoms, which leads to the inclined columnar growth towards the Co source. This shadowing model of growth was already postulated by Smith [3]. The Cr atoms, which form the minor evaporation flux, come from an opposite direction, and thus have the shadowed area in the opposite direction of the Co. They are most likely to impinge at the Co shadowed-area-side at every stage of the growth. With limited mobility (especially with the T_R-samples), the adatoms will not have sufficient energy to move around to find the energetically most favourable places. This results in the so-called process-induced compositional separation, in which one side of the columns is Cr-rich. At a higher substrate temperature more surface diffusion will take place and transition to the thermally enhanced compositional separation occurs. [2]

Simulations.

The above-mentioned growth model is implemented in a 2D-Monte Carlo simulation program [4]. Figure 5 shows two simulation results, one for low diffusion (comparable to the T_R-samples), the other at higher diffusion (comparable to the T_H-samples). These figures clearly show the enhanced Cr distribution at one side of the columns with low diffusion and more intermixing of Co and Cr at higher diffusion. They also show larger columnar sizes at higher diffusion.

NMR and AES analysis.

NMR analysis supports the existence of highly separated regions. Recently for sputtered Co-Cr films NMR results have been reported in [5]. In the T_R-samples a nearly pure Co component is found to exist, which can only be caused by the process geometry because the deposition temperature is far too low to cause thermally enhanced compositional separation. Fig. 6 shows a measured spin-echo spectrum. The peak at 222 MHz is due to a highly pure Co component. The small increase in intensity around 170 MHz is due to a small amount of Co surrounded by 1 Cr next neighbour [5,6]. The peak at 120 MHz is due to a Co-oxide. Further NMR results will be discussed in [7].

The T_H-samples show similar spectra. The main difference is the slight shift of the main frequency from 222 MHz to 218-219 MHz. This means that there is a highly Co-rich component (with about 5 at%Cr) in the T_H-films.

The existence of oxygen in the films also became clear from an Auger depth profile measured for the 250-nm T_R-sample.

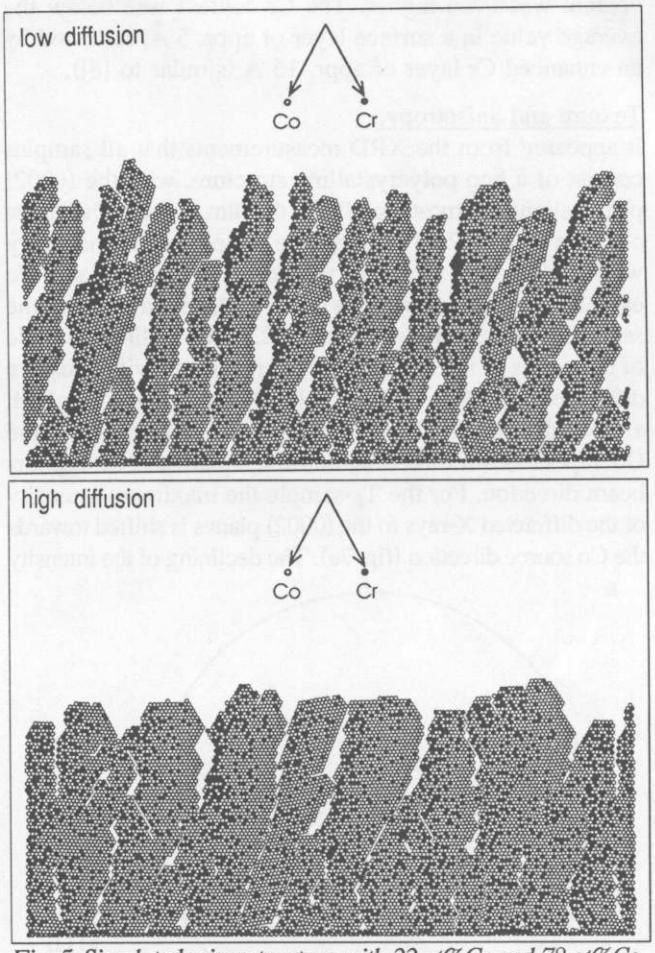

Fig. 5. Simulated microstructure with 22 at%Cr and 78 at%Co.

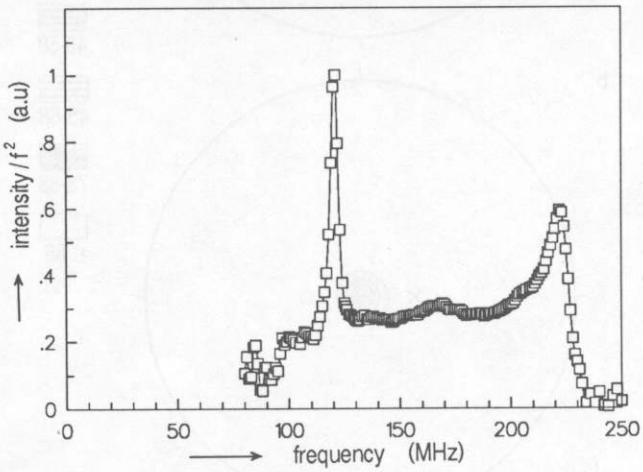

Fig. 6. NMR spectra of the 400 nm thick T_R-sample.

We measured an oxygen content of appr. 5% throughout the whole film. In a surface layer of 150 Å thick the oxygen

content was even higher. The Cr content was below the average value in a surface layer of appr. 5 Å, followed by an enhanced Cr layer of appr. 15 Å (similar to [8]).

Texture and anisotropy.

It appeared from the XRD measurements that all samples consist of a hcp polycrystalline structure, with the (0002) planes aligned (almost) parallel to the film surface. The lattice constant $d_{(0002)}$ is 2.03 Å. For some samples we found a very weak (100) and an even weaker (101) reflection. We calculated a=2.50 Å and thus c/a=1.624, which is nearly the same as for pure hcp ε-Co (c/a=1.623). The inclination angle of the c-axis of the hcp structure is measured with a texture diffractometer. Fig. 7 shows a {0002} pole figure for both a T_R- and a T_H-sample. In this figure the cross indicates the Co vapour-beam direction, and the square the Cr vapour-beam direction. For the T_R-sample the maximum intensity of the diffracted X-rays to the (0002) planes is shifted towards the Co source direction (fig. 7a). The declining of the intensity

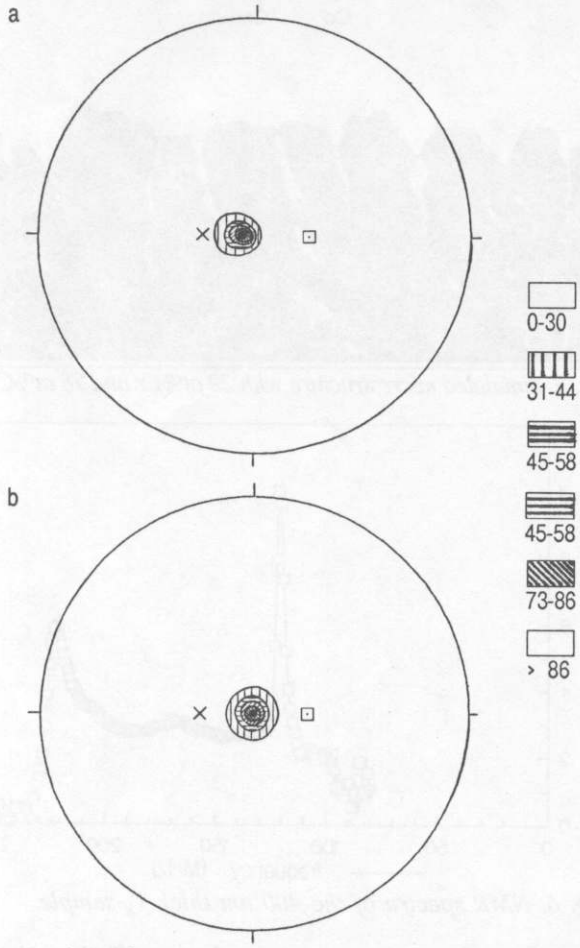

Fig. 7. {0002} pole figures; a) T_R-sample; b) T_H-sample. The pole density is plotted on a scale from 0-100%.

is a-symmetrical. As typical inclination angles of the c-axis (γ_{c1}) we measured values of between 5° and 9° for the T_R-samples; typical values for the T_H-samples were between 0° and 5°. As an illustration see figure 7b, where the maximum intensity is around the film normal. For the thicker T_R-samples we measured an increasing number of {20$\bar{2}$3} planes ∥ film surface, thus giving a second tilt angle of the c-axis of appr. 45° towards the Cr source. This becomes significant for film thicknesses larger than 350 nm. No second c-axis was measured for the T_H-samples.

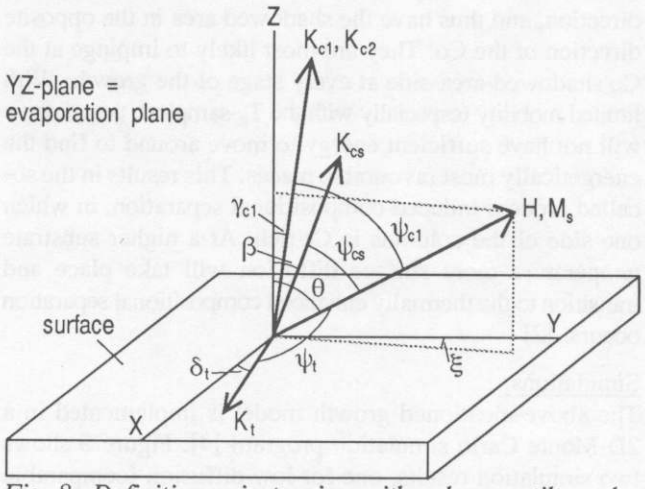

Fig. 8. Definition anisotropies, with columnar tilt angle β and c-axis tilt angle γ_{c1}.

The magnetic anisotropy consists of several contributions. The main one is hcp crystalline anisotropy with constants K_{c1} and K_{c2} parallel to the c-axis, see fig. 8. The magnetocrystalline energy per unit volume is given in formula 1, which is cut after the second term:

$$E_c = K_{c1}\sin^2\psi_{c1} + K_{c2}\sin^4\psi_{c1} + \ldots \quad \{1\}$$

K_{c2} is appr. 5% (10%) of K_{c1} for the T_R- (T_H-) samples. K_{c3} is negligibly small with respect to K_{c1} and K_{c2}. A typical value is K_{c1} = 100 kJm^{-3} (T_R). Off-centre samples have the same crystalline anisotropies.

Microstructure and anisotropy.

A smaller contribution to the anisotropy is given by columnar shape anisotropy with constant K_{cs} along the columnar axis. This is possibly due to the high degree of separation of Co and Cr as explained earlier, which gives some degree of decoupling of magnetic spins at the column boundaries. The columnar shape anisotropy gives rise to an energy:

$$E_{cs} = K_{cs}\sin^2\psi_{cs} \quad \{2\}$$

We found a slight trend of increasing tilt angle of the columnar axis, β, with increasing film thickness: from 12° (250 nm) to 15° (750 nm) for the T_R-samples. The columnar tilt angle

is smaller for the T_H-samples, which is due to higher surface diffusion: β = 7° (250 nm) to 10° (750 nm). One example of a SEM micrograph, where it is possible to see the inclined columnar structure is given in figure 9.

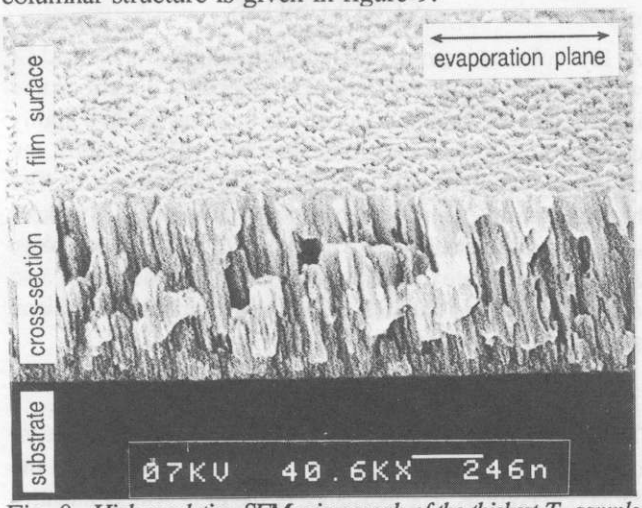

Fig. 9. High resolution SEM micrograph of the thickest T_H-sample (tilt in SEM: 20°).

The columnar tilt angle β is larger than the c-axis tilt angle γ_{cl}. Due to this a lot of stacking faults can be expected [9], which in turn leads to a high half width value of the rocking curve $\Delta\theta_{50}$. We measured $\Delta\theta_{50}$ around 16°.

A transversal in-plane anisotropy was found from the in-plane torque measurements with constant K_t and direction perpendicular to the evaporation plane (δ_t=0° in fig. 8). Its contribution to the anisotropy energy (per unit volume) is:

$$E_t = K_t \sin^2\psi_t \qquad \{3\}$$

K_t increases strongly with film thickness: from 15 kJm^{-3} (50 nm film) to 40 kJm^{-3} (750 nm). Since K_t is larger than the projection of $K_1+K_2+K_{cs}$ in the film plane, the effective in-plane anisotropy direction is perpendicular to the evaporation plane.

High resolution SEM observations of the samples revealed small columns which form bundles perpendicular to the evaporation plane. The shape anisotropy of the bundles contributes to K_t. Besides the bundles, stress also contributes to the in-plane anisotropy. Figure 10 shows the largest structures on the surface that we observed. In fig.10a we see a T_R-sample with bundles, i.e. clustering of columns in a direction perpendicular to the evaporation plane. In the direction parallel to the evaporation plane the columns are separated by voids which arise due to the shadowing mechanism. Perpendicular to the evaporation plane this shadowing is not present. In this direction there is a continous supply of vapour material thus giving no rise to (large) separations in between the columns. The T_H-samples show different surface structures with the development of hexagonal shape-like columns, see fig. 10b (arrow), and bundles cannot be distinguished. Earlier results for a series deposited at a rate twice as high [2] also showed the hexagonal shape of the columns for the high temperature samples. However, the bundles were not observed. For oblique evaporation from one source, the formation of bundles is also dependent on the deposition rate [10].

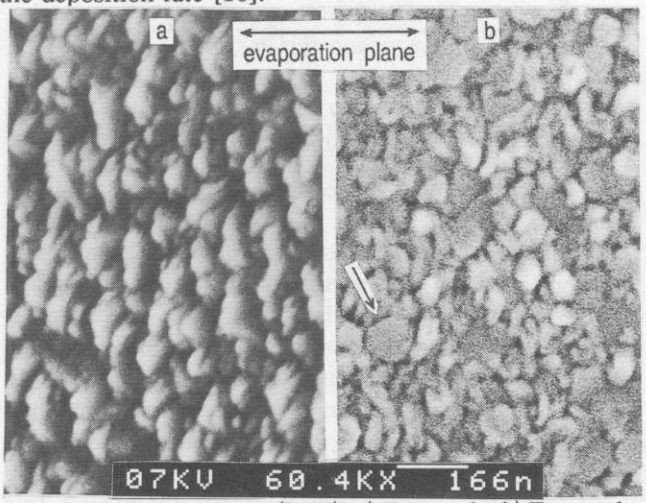

Fig.10. Surface structure (SEM); a) T_R-sample; b) T_H-sample.

Columnar dimensions measured from the surface SEM observations are as follows (the film thickness is given in brackets): For the T_R-samples: 12-25 nm (250 nm) and 15-35 nm (400 and 750 nm). For the T_H-samples: 12-30 nm (250 nm) and 15-50 nm, hexagonal shape (400 nm) and 15-110 nm, hexagonal shape (750 nm). The surface roughness is high and increases with film thickness. The roughness is inherent to the shadowing mechanism and is a disadvantage in recording, because it increases the noise level.

For the effective easy axis of the magnetization, also the film demagnetization, K_d contributes:

$$K_d = \frac{1}{2}\mu_0 M_s^2 \cos^2\theta \qquad \{4\}$$

Formulae 1 to 4 are used to derive an expression for the torque. A Fourier expansion is carried out, similar to [11]. The Fourier coefficients are split up for the 3 different measurement planes LM, TM and IP, see fig. 2. The measured Fourier coefficients are extrapolated to infinite field to correct for the angle between the applied field and the magnetization. The extrapolated coefficients are set equal to the calculated ones. In addition we use the angle β as determined from cross-sectional SEM and the angle γ_{cl} as measured with XRD. We present the results in relation to the total effective out-of-plane anisotropy K_e, which has a tilt angle γ. Typical values for the 250 nm thick T_R (T_H) samples are: K_e = 120 (150) kJm-3,

γ = 8° (4°) and K_{c2} = 5% (7%) of K_u. The estimation of the share of K_{c1} and K_{cs} is very inaccurate due to its large sensitivity to the angles β and γ_{c1}. For instance a variation of 1° in γ_{c1} gives a 10% difference in the share of K_{c1} and K_{cs}. We found $K_{cs} \leq 35\%$ of K_u and $K_{c1} \geq 65\%$ of K_u for both the T_R and T_H-samples.
We use a quality factor as defined in formula 5:

$$Q_\perp = \frac{\Sigma \textit{ perpendicular anisotropy energies}}{\Sigma \textit{ in-plane anisotropy energies}} = \frac{(K_{c1}+K_{c2})\cos\gamma_{c1} + K_{cs}\cos\beta}{K_d\cos\gamma + K_t + (K_{c1}+K_{c2})\sin\gamma_{c1} + K_{cs}\cos\beta} \qquad \{5\}$$

For our samples $Q_{\perp,LM}$ was measured at appr. 0.9-1 and $Q_{\perp,TM}$ at appr. 0.8-0.9. Of course, it should be realised that in recording the head field does not saturate the sample, and the sample's state of demagnetization at this field is important for the quality factor. Especially $Q_{\perp,LM}$ is of importance if a ring head is used for recording. With the head-medium movement in the LM direction the tilted easy axis is an advantage. Due to the different sensitivity of the medium to the leading and the trailing edge of the head the frequency response has fewer additional minima [12]. For the off-centre samples we get a variation in the quality factor by ±0.2. This is caused by the variation in M_s and thus in K_d.

Angle dependent coercivity and hysteresis loss.

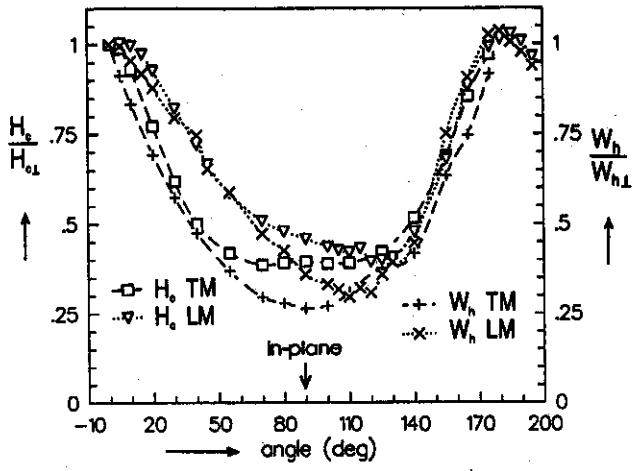

Fig. 11. Angle dependent behaviour of H_c and W_h.

We performed angle dependent VSM measurements to learn more about the reversal mechanism of the magnetization. Figure 11 shows $H_c(\alpha)$ and $W_h(\alpha)$, with α measured from the film normal, see fig. 2. The tilted out-of-plane easy axis towards the Co-source direction is expressed by the fact that the maximum coercivity and maximum hysteresis loss are at different angles for the LM and TM measurements [2].

The strong decreases of both the coercivity and the hysteresis loss towards the in-plane direction indicate a rotational reversal of the magnetization and much pinning of domain walls occurs.

CONCLUSIONS

At low substrate temperature the combination of Co and Cr which arrive at the substrate from opposing directions and insufficient diffusion of deposited atoms results in a highly compositional separated microstructure. This enables the deposition of media with good magnetic characteristics. The high degree of Co and Cr separation was qualitatively found in the simulation studies and is proved by the NMR experiments. At higher substrate temperature a Co-Cr alloy develops, also due to diffusion, and transition to thermally enhanced compositional separation takes place.

ACKNOWKLEDGEMENTS

The authors are obliged to Mr. T. Masuda for doing the Auger depth profiling and to Mr. A.M. Otter for carrying out the SEM observations. The assistance of the EC CAMST initiative is also acknowledged.

REFERENCES

1. F.A. Pronk and J.C. Lodder, IEEE Trans. Mag., vol. MAG-24, pp 1744-1747, 1988.
2. H. van Kranenburg, J.C. Lodder, Y. Maeda, L. Toth and Th.J.A. Popma, IEEE Trans. Mag., vol. MAG-26, pp 1620-1622, 1990.
3. D.O. Smith, M.S. Cohen and G.P. Weiss, J. Appl. Phys., vol 31, pp 1755-1762, 1960.
4. S. Müller-Pfeiffer, H. van Kranenburg and J.C. Lodder, to be published.
5. K. Takei and Y. Maeda, Jap. J. Appl. Phys. Letters, vol 30, pp L1125-L1128, 1991.
6. K. Yoshida, H. Kakibayashi and H. Yasuoka, J. Appl. Phys. vol. 68, pp 705-712, 1990.
7. J.C. Lodder, H. van Kranenburg, K. Takei and Y. Maeda, to be published.
8. T. Masuda, W. Geerts and J.C. Lodder, J. Magn. Magn. Mat., vol 95, pp 123-132, 1991.
9. U. Hwang, Y. Uchiyama, K. Ishibashi and T. Suzuki, Thin Solid Films, pp 231-241, 1987.
10. K. Okamoto, T.Hashimoto, K. Hara, M. Kamiya and H. Fujiwara, Thin Solid Films, vol. 147, pp 299-311, 1987.
11. S. Swaving,G.J. Gerritsma, J.C. Lodder and Th.J.A. Popma, J. Magn. Magn. Mat., vol 67, pp 155-164, 1987.
12. J.P.C. Bernards, G.J.P. van Engelen, C.P.G. Schrauwen, H.A.J. Cramer and S.B. Luitjens, IEEE Trans. Mag., vol. MAG-26, pp 2289-2291, 1990.